

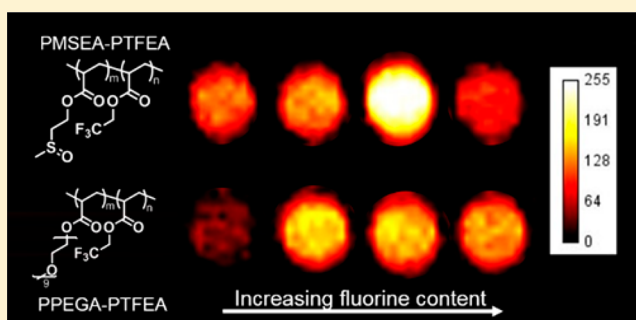
Enhanced Performance of Polymeric ^{19}F MRI Contrast Agents through Incorporation of Highly Water-Soluble Monomer MSEA

Changkui Fu,^{†,‡} Cheng Zhang,^{†,‡} Hui Peng,^{†,‡} Felicity Han,[†] Carly Baker,[†] Yuao Wu,[†] Hang Ta,^{†,§} and Andrew K. Whittaker^{*,†,‡,§}

[†]Australian Institute for Bioengineering and Nanotechnology and [‡]ARC Centre of Excellence in Convergent Bio-Nano Science and Technology, The University of Queensland, Brisbane, QLD 4072, Australia

Supporting Information

ABSTRACT: ^{19}F magnetic resonance imaging (MRI) is a powerful noninvasive imaging technique that shows tremendous potential for the diagnosis and monitoring of human diseases. Fluorinated compounds are commonly used as ^{19}F MRI contrast agents to develop “hot spot” imaging. To achieve high-resolution MR images, a high density of ^{19}F nuclei is required in the contrast agents. However, because of the inherent hydrophobicity of fluorinated moieties, aggregation of ^{19}F contrast agents with high fluorine content is often observed in aqueous solution, resulting in attenuated MR signal and low sensitivity, thus significantly limiting their further biological applications. Here we report the synthesis and characterization of a series of polymeric ^{19}F MRI contrast agents with high fluorine content by copolymerizing the well-known fluorinated monomer 2,2,2-trifluoroethyl acrylate (TFEA) with a highly water-soluble monomer 2-(methylsulfinyl)ethyl acrylate (MSEA) using RAFT polymerization. We show that these polymeric contrast agents, although with high fluorine content, display remarkable imaging performance as evidenced by preferable relaxation properties and intense *in vitro/in vivo* MRI signals, demonstrating the huge potential for eventual clinical applications such as MRI-guided disease diagnosis and therapy.



INTRODUCTION

Over the past few decades, magnetic resonance imaging (MRI) has been widely used in the clinic for disease diagnosis and monitoring of treatment due to advantages such as non-invasiveness, deep-tissue penetration, and excellent spatial resolution (submillimeter).¹ To better highlight the anatomical and pathological features of the tissue of interest, contrast agents are often required to improve the sensitivity of the MRI scan by enhancing the image contrast.² Paramagnetic or superparamagnetic metal-ion-based compounds such as gadolinium chelates and iron oxide nanoparticles have achieved large success as ^1H MRI contrast agents.^{3–5} These agents can modulate the relaxation properties of nearby water molecules to induce additional contrast, allowing significantly improved visualization of the region of interest. Despite their success in the clinic, the metal-based contrast agents present several inherent disadvantages. Principally, the agents alter the relaxation properties of the surrounding water protons and hence are only detected indirectly. Hence, quantitative analysis is difficult. Also, the ubiquitous large content of water in tissues results in significant background signal interference, making it at times difficult to identify the target tissue. In addition, safety concerns are associated with the use of metal-based contrast agents. For example, gadolinium-based contrast agents have been reported to be involved in the development of

nephrogenic systemic fibrosis in patients with impaired kidney function.^{6,7} Gadolinium-based contrast agents can be retained in body including the brain for months or even years as warned by the US FDA recently.⁸ The long-term retention of gadolinium is potentially a concern for both healthcare professionals and patients.

A strategy to overcome the limitations of ^1H MRI is to develop probes based on nuclei other than the proton.^{9–12} ^{19}F MRI is a promising alternative to ^1H MRI due to the favorable NMR properties of ^{19}F such as large gyromagnetic ratio and high natural abundance. Fluorinated compounds are of course required as contrast agents for ^{19}F MRI.^{13,14} In contrast to ^1H MRI contrast agents that affect the relaxation properties of nearby water molecules without being visualized directly, ^{19}F MRI contrast agents have an innate MR signal comparable to ^1H MRI to create “hot spot” images which are not obscured by the large pool of protons in the biological system.^{15–18} Furthermore, thanks to the lack of endogenous MRI-detectable fluorine in the human body, a linear relationship between ^{19}F content and the MR intensity can be expected, allowing for quantitative applications in cell tracking for immunother-

Received: June 5, 2018

Revised: July 16, 2018

Published: July 26, 2018

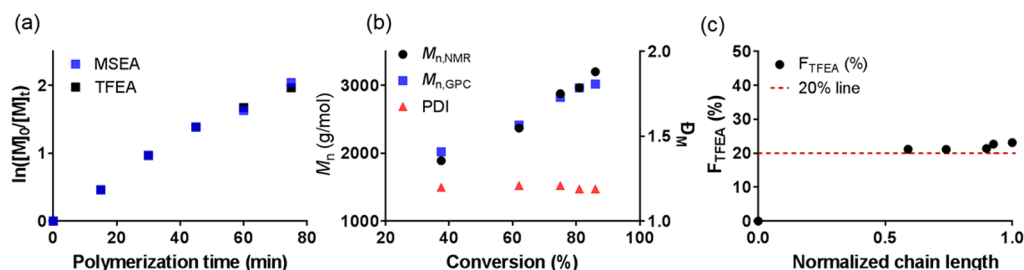
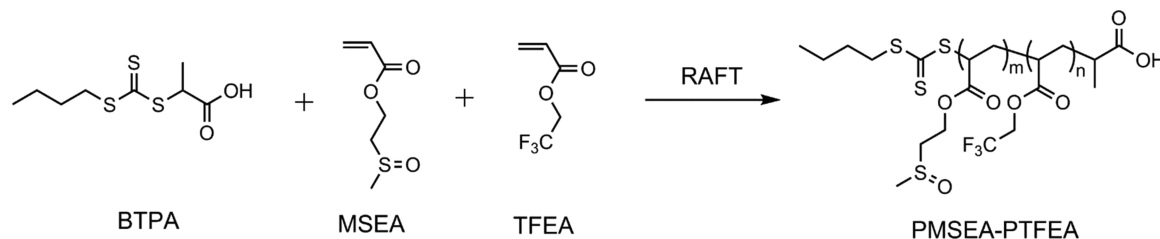
Scheme 1. RAFT Synthesis of Polymeric ^{19}F MRI Contrast Agents via Copolymerization of MSEA with TFEA

Figure 1. (a) Pseudo-first-order kinetic plot of the conversion of MSEA and TFEA against polymerization time. (b) Evolution of molecular weight and dispersity with total monomer conversion. (c) Dependence of cumulative mole fraction of TFEA in the polymer on the normalized chain length during the RAFT copolymerization of MSEA and TFEA.

apy.^{19–21} The design of ^{19}F contrast agents is crucial for ^{19}F MRI. To enable the sensitivity of ^{19}F MRI suitable for biological application, ^{19}F contrast agents with a high density of ^{19}F are preferred. However, due to the inherent hydrophobicity of fluorine, aggregation of ^{19}F contrast agents with high fluorine content is often observed in aqueous solution, resulting in attenuated MR signal and low sensitivity, thus significantly limiting their further biological applications.²² Highly fluorinated compounds such as perfluorocarbons (PFCs) or perfluoropolyethers (PFPE) have been used to fabricate ^{19}F MRI contrast agents with high fluorine content.^{23–25} Because of the highly hydrophobic nature of PFC and PFPE, they are normally formulated as nano-emulsions for ^{19}F MRI applications. However, these nano-emulsions are not stable upon prolonged storage²⁶ and show a feature of long biological half-life (several weeks),²⁷ which is not preferable for clinical use. Simply fluorinated molecules can also be used to construct ^{19}F MRI contrast agents with diverse functionality, good stability, and magnetically equivalent fluorine atoms compared to PFC- or PFPE-based nano-emulsions.^{28,29} For example, our group and others have developed a number of polymeric ^{19}F MR contrast agents by copolymerizing 2,2,2-trifluoroethyl (meth)acrylate (TFE(M)-A) with hydrophilic monomers such as poly(ethylene glycol) methyl monoether (meth)acrylate (PEG(M)A).^{30–35} By careful design, these polymeric fluorinated polymers can be prepared with excellent biocompatibility, tunable sizes, and tailored functionalities to meet the requirements of various applications. However, these partly fluorinated polymers often possess low fluorine content (normally below 5 wt %) that can only produce moderate MRI signals. Further increasing fluorine content within the polymers would reduce rather than increase the MRI sensitivity as a consequence of severe aggregation of fluorine moiety causing strong dipolar couplings of the ^{19}F spins. This becomes a major obstacle preventing current fluorinated polymers from further *in vivo* use.

Sulfoxide-containing polymers have attracted increasing attention due to their excellent water solubility owing to the strong hydrophilicity of the sulfinyl group.^{36,37} The sulfinyl

group can be readily obtained by oxidation of thioether, which is often used for the construction of oxidation-responsive polymeric systems.^{32,38–42} In this contribution, we report the synthesis and characterization of a series of polymeric ^{19}F MRI contrast agents with various fluorine contents by copolymerizing extensively studied fluorinated monomer 2,2,2-trifluoroethyl acrylate (TFEA) with a highly water-soluble sulfoxide-containing monomer 2-(methylsulfinyl)ethyl acrylate (MSEA) using reversible addition–fragmentation chain transfer (RAFT) polymerization (Scheme 1). Thanks to the low molecular weight ($M_w = 162.2$) and high hydrophilicity of MSEA, fluorinated polymers with high weight percentage of fluorine (5.8–19.3 wt %) and good water solubility can be readily obtained. Further NMR and MRI studies reveal that these polymeric contrast agents, although possessing high fluorine content, can retain remarkable imaging performance as evidenced by desirable relaxation properties and intense MRI signal, demonstrating their large potential for future biological applications.

RESULTS AND DISCUSSION

RAFT polymerization was chosen for the synthesis of the polymeric ^{19}F contrast agents given its applicability to a diverse range of monomer families, excellent functional group tolerance, and ease of work-up. A RAFT polymerization with a ratio of [BTPA]:[AIBN]:[MSEA]:[TFEA] = 1:0.1:20:5 in DMF at 70 °C was set up initially. Kinetic studies were carried out to investigate the RAFT copolymerization of MSEA and TFEA. As shown in Figure 1a, the polymerization of both MSEA and TFEA followed linear pseudo-first-order kinetics, indicating a relatively constant rate of monomer consumption throughout the polymerization. A comparison of conversion of MSEA and TFEA suggests that the two monomers react at similar rates. The molecular weight of the polymer increased linearly while the dispersity remained narrow as the polymerization proceeded (Figure 1b), indicative of a well-controlled polymerization process. In addition, the mole fraction of TFEA in the polymer throughout polymerization remained constant at ~20% in line with the monomer feed ratio (MSEA:TFEA,

20:5), demonstrating that a statistical copolymer of MSEA and TFEA was formed (Figure 1c). The resultant polymer was further characterized by NMR. The ^1H NMR spectrum revealed the characteristic peaks due to MSEA and TFEA (Figure 2). The CH_2 adjacent to the ester bond of both

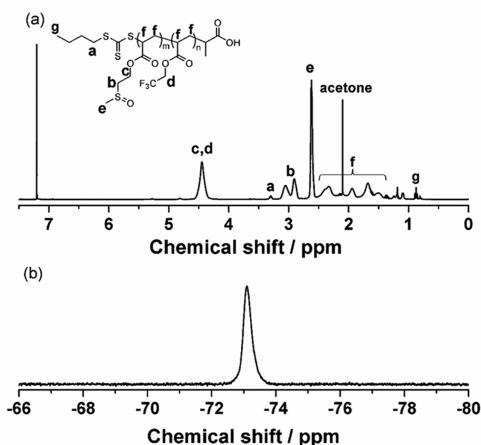


Figure 2. (a) ^1H NMR (CDCl_3) spectrum and (b) ^{19}F NMR (D_2O) spectrum of PMSEA–PTFEA.

monomers appeared at 4.45 ppm (c, d) while the CH_3 and CH_2 near the sulfur atom of MSEA can be observed at 2.82–3.16 ppm (b) and 2.62 ppm (e), respectively. The peaks due to the backbone of the polymer can be found at 1.36–2.50 ppm (f). The characteristic peaks corresponding to the CH_2 next to the trithiocarbonate and the terminal CH_3 of RAFT agent can be also seen at 3.30 ppm (a) and 0.87 ppm (g). Furthermore, ^{19}F NMR of PMSEA–PTFEA in D_2O was conducted and revealed a single intense peak at -73.2 ppm due to the presence of TFEA units, which is important for subsequent NMR and MRI studies. To investigate the effect of fluorine content on the NMR and MRI properties of polymeric ^{19}F contrast agents, a series of PMSEA–PTFEA copolymers with various ^{19}F content ranging from 5.8 to 24.7 wt % were prepared using the above-described method. For comparison,

copolymers of PEGA and TFEA (PPEGA–PTFEA) with comparable fluorine contents were also prepared. The structure and property details on all the polymers are listed in Table 1.

The solubility of the PMSEA–PTFEA polymers was investigated by dissolving the polymers in PBS buffer (pH = 7.4). The polymers with 5.8–15.3 wt % fluorine could be readily dissolved in PBS without the addition of organic solvents as solubilizers. Further increases in the fluorine content resulted in poor solubility. For instance, the polymer with 19.3 wt % fluorine dissolved slowly in PBS. The polymer with a higher fluorine content of 24.7 wt % could not be dispersed in PBS due to severe aggregation. ^1H DOSY NMR was used to determine the size of the polymers in aqueous solution. As shown in Table 1, the hydrodynamic radii of the polymers estimated from ^1H DOSY NMR are rather small (below 5 nm), consistent with the number-based sizes given by DLS. While the DLS data based on intensity showed two peaks, the DLS data based on number displayed only one peak with size below 10 nm (Figure S1). This indicates that the population giving the second peak at over 100 nm in the intensity-based distribution is small. The second peak in the intensity-based distribution can be attributed to agglomerated polymer chains due to lack of swelling in water.⁴³ It is also observed that although all the PMSEA–PTFEA polymers have comparable molecular weights, the size of these polymers in aqueous solution increased with increasing fluorine content. This is evidence of aggregation of the polymers with higher fluorine contents. The aggregation of the polymers was also reflected in the gradual line broadening of the single peak in the ^{19}F NMR spectra of the polymers with increasing fluorine content (Figure 3).

^{19}F MRI contrast agents require not only a relatively high fluorine content but also favorable spin–lattice relaxation (T_1) and spin–spin relaxation (T_2) properties. To achieve a higher intensity MR image, short T_1 and long T_2 times are preferred. The relaxation times of the polymers in PBS solution were measured at a field strength of 9.4 T. As shown in Table 1 and Figure 4, the T_1 and T_2 times of PMSEA–PTFEA and PPEGA–PTFEA polymers were found to be dependent on the fluorine content. Both the T_1 and T_2 times decreased with

Table 1. Details of Polymeric ^{19}F Contrast Agents Prepared by RAFT Copolymerization

entry	$[\text{MSEA}]_0:[\text{TFEA}]_0$ feed ratio	^{19}F content ^a (wt %)	$M_{n,\text{GPC}}^b$ (g/mol)	$M_{n,\text{NMR}}^c$ (g/mol)	D_M^b	R_h^d (nm)	D_h^e (nm)	ζ^e (mV)	T_1 (ms)	T_2 (ms)
1	20:5	5.8	3320	3930	1.29	1.44	2.1	-4.0 ± 0.7	641	330
2	20:10	9.7	3450	4710	1.34	1.69	3.5	-12.6 ± 1.6	556	215
3	15:15	15.3	3130	3720	1.28	2.45	5.2	-16.9 ± 1.7	453	100
4	15:20	19.3	4250	5910	1.26	5.00	7.2	-11.6 ± 0.8	444	22
5	10:20	24.7	3960	4610	1.25					
entry	$[\text{PEGA}]_0:[\text{TFEA}]_0$ feed ratio	^{19}F content ^a (wt %)	$M_{n,\text{GPC}}^b$ (g/mol)	$M_{n,\text{NMR}}^c$ (g/mol)	D_M^b	R_h^d (nm)	D_h^e (nm)	ζ^e (mV)	T_1 (ms)	T_2 (ms)
6	20:15	6.0	9720	12320	1.13	2.59	2.7	-6.7 ± 0.8	459	139
7	15:20	10.0	7000	10840	1.13	2.91	5.5	-10.3 ± 1.7	432	73
8	8:20	16.1	4140	6370	1.17	4.26	8.0	-13.3 ± 1.3	423	36
9	5:21	18.5	5240	4310	1.11	4.90	8.3	-10.2 ± 2.5	427	28

^aCalculated by ^1H NMR following the equation $^{19}\text{F}\% = \text{DP}_{\text{TFEA}} \times 3 \times 19 / M_{n,\text{NMR}}$ where $M_{n,\text{NMR}}$ is the molecular weight of the polymer given by NMR. ^bCalculated by DMAc GPC for PMSEA–PTFEA polymers or THF GPC for PPEGA–PTFEA polymers. ^cCalculated by ^1H NMR following the equation $M_{n,\text{NMR}} = \text{DP}_{\text{TFEA}} \times M_{w,\text{TFEA}} + \text{DP}_{\text{MSEA}} \times M_{w,\text{MSEA}} + M_{w,\text{BTFA}}$. ^dCalculated by ^1H DOSY NMR based on the Stokes–Einstein equation $R = kT / 6\pi\eta D$, where k is the Boltzmann constant, T is the experimental temperature (298 K), η is the viscosity of water (8.90×10^{-4} Pa), and D represents the diffusion coefficient of the polymer measured by ^1H DOSY NMR. ^eDetermined by DLS. For the DOSY NMR and DLS studies, the concentration of polymers was 10 mg/mL in PBS.

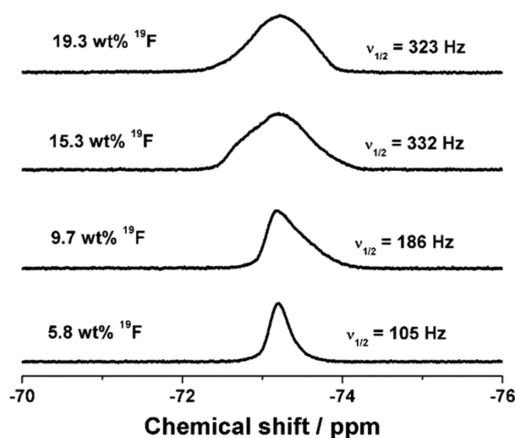


Figure 3. ^{19}F NMR (D_2O) spectra of polymers with different fluorine contents (concentration = 10 mg/mL).

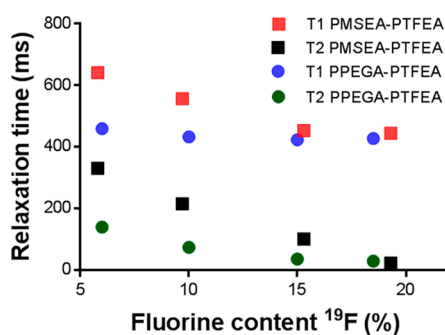


Figure 4. Dependence of relaxation times of the polymers on the fluorine content.

increasing fluorine content in the polymers. Generally, PMSEA–PTFEA polymers had longer T_1 and T_2 times in comparison with PPEGA–PTFEA polymers. However, at high fluorine contents approximating 19 wt %, the two classes of copolymers displayed comparable T_1 and T_2 times.

Solutions of the copolymers were imaged to demonstrate the applicability of the polymers as ^{19}F MRI contrast agents. ^{19}F MR images of the polymers with a range of fluorine contents were successfully acquired at a polymer concentration of 10 mg/mL in PBS solution (Figure 5). The ^{19}F MRI signal intensity (or the signal-to-noise ratio (SNR)) of all the polymers increased with increasing fluorine content up to 15 wt % (Figure 5b). However, the polymer with highest fluorine content (~ 19.3 wt %) displayed a decreased ^{19}F MRI signal intensity. In contrast, PPEGA–PTFEA polymers showed the highest signal intensity when the fluorine content was 10 wt %. Further increases in fluorine content within the PPEGA–PTFEA polymers resulted in a progressive decrease in image intensity. In summary, the copolymers incorporating MSEA have a significantly higher maximum MRI signal, indicating that this monomer is able to more effectively screen the fluorinated TFEA monomers and prevent strong dipolar interactions to higher fluorine contents compared with the PPEGA–PTFEA polymers.

The effect of concentration on the properties of PMSEA–PTFEA was also investigated. The polymer with 15.3 wt % fluorine content showing the highest MRI intensity was selected for these studies. As shown in Figure 6a, with an increase in polymer concentration in solution, the self-diffusion coefficient decreased slightly. This indicates that the hydro-

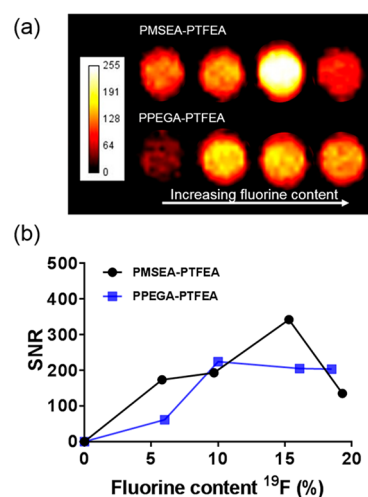


Figure 5. (a) ^{19}F MRI images of solutions of PMSEA–PTFEA and PPEGA–PTFEA copolymers. (b) Dependence of SNR on the fluorine content of the polymers.

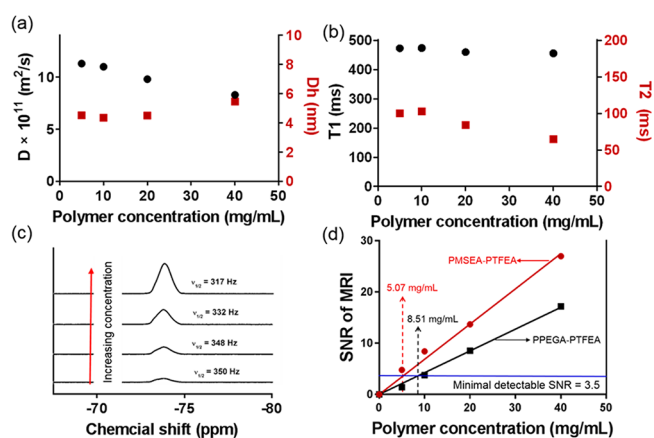


Figure 6. Dependence of diffusion coefficient and hydrodynamic diameter D_h (a), NMR relaxation times (b), ^{19}F NMR spectra (c), and ^{19}F MRI SNR (d) on the concentration of polymer in solution.

dynamic diameter of polymers only underwent a small increase and that no large aggregates were formed with polymer concentration up to 40 mg/mL. The NMR relaxation times of the polymers at different polymer concentrations are plotted in Figure 6b. The slight decrease in T_2 relaxation times is expected from theory as the solution viscosity increases. T_1 , on the other hand, is almost invariant with concentration, indicating that the spectral density of high-frequency motions responsible for longitudinal relaxation does not change significantly and/or the solutions are close to the minimum in T_1 relaxation times. No strong line broadening of the ^{19}F NMR spectrum was observed with increased polymer concentration (Figure 6c), and the NMR intensity displayed a linear dependence on polymer concentration (Figure S2). MRI measurements also revealed that the SNR increased linearly with increasing polymer concentration (Figure 6d). The linear relationship between NMR/MRI intensity and the concentration of the fluorinated polymers is important for use of these molecules in quantitative ^{19}F MRI studies. In addition, if we propose a minimum detectable SNR as 3.5 as suggested in previous studies,^{44,45} the detection limit for this PMSEA–PTFEA polymer is determined as ~ 5 mg/mL by linear extrapolation of the relationship between SNR and polymer

concentration. This is much lower than the detection limit (8.5 mg/mL) for the PPEGA–PTFEA polymer.

Low cytotoxicity is crucial for biological applications of contrast agents. The cytotoxicity of PMSEA–PTFEA polymer was studied by measuring the cell viability of CHO cells after incubation for 24 h in the presence of solutions of the copolymers. As shown in Figure 7, the CHO cells maintained a

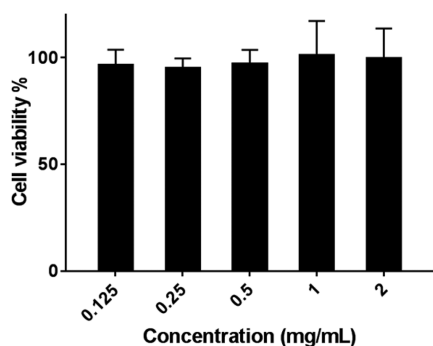


Figure 7. Viability of CHO cells in the presence of different concentrations of PMSEA–PTFEA polymer with 15.3 wt % fluorine.

very high viability at concentrations of polymer up to 2 mg/mL, indicating that PMSEA–PTFEA displays good biocompatibility and is suitable for further biological applications.

The potential for the PMSEA–PTFEA polymers to be used for *in vivo* animal imaging was subsequently examined. 200 μ L of solution of a polymer with 15.3 wt % fluorine at a concentration of 40 mg/mL was injected to mice through the tail vein. Figure 8a showed the overlaid $^1\text{H}/^{19}\text{F}$ MR images of a

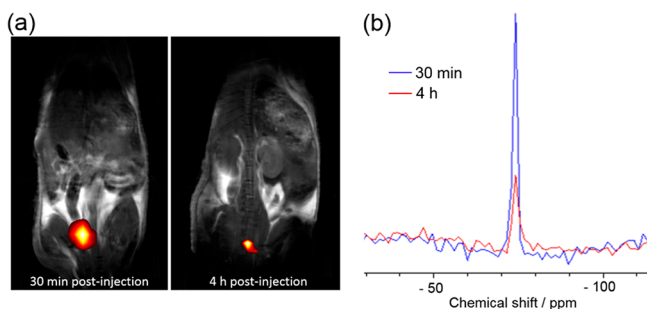


Figure 8. (a) *In vivo* $^1\text{H}/^{19}\text{F}$ MRI (coronal view) at 9.4 T of a mouse following injection with PMSEA–PTFEA with 15.3 wt % ^{19}F . (b) *In situ* NMR spectra of the mouse at 30 min and 4 h postinjection.

mouse acquired at 30 min and 4 h postinjection. The ^{19}F MRI signal can be clearly observed in the mouse after scanning for a short time (~ 13 min). Because of the small size of the polymer ($D_h \sim 5.5$ nm), the polymer underwent rapid clearance, and the ^{19}F MRI signal was observed in the bladder of the mouse at 30 min postinjection. At 4 h postinjection, the ^{19}F signal decreased significantly due to excretion from the bladder. Whole-body ^{19}F NMR spectra were also collected to monitor the change of ^{19}F intensity postinjection. As can be seen in Figure 8b, the ^{19}F NMR intensity decreased obviously at 4 h postinjection compared with that at 30 min postinjection, in good agreement with the MRI result. Based on these preliminary *in vivo* results, the PMSEA–PTFEA polymers have excellent ^{19}F MR imaging properties showing high resolution and sensitivity. It also needs to point out that the *in vivo* circulation time of polymeric ^{19}F MRI contrast agents is

highly dependent on their size, which is to a great extent determined by molecular weight. Thus, we can simply vary the molecular weights of synthesized fluorinated polymers to tune the *in vivo* circulation behavior. For future applications requiring longer circulation time, we can potentially use PMSEA–PTFEA polymers with higher molecular weights.

In conclusion, we have developed a new class of polymeric ^{19}F MRI contrast agents by combining the highly hydrophilic monomer MSEA with the fluorinated monomer TFEA by RAFT polymerization. These ^{19}F MRI contrast agents have significantly higher fluorine content (5.8–19.3 wt %) compared with previously reported partly fluorinated polymer imaging agents with fluorine content normally below 5 wt %. A comparison between synthesized PMSEA–PTFEA and PPEGA–PTFEA polymers on relaxation properties as well as ^{19}F MRI imaging has been made. The PMSEA–PTFEA polymers showed a significantly higher maximum MRI signal intensity at a fluorine content of 15.3 wt % whereas the PPEGA–PTFEA polymers had a maximum signal intensity with relatively lower SNR at a fluorine content of 10.0 wt %. The PMSEA–PTFEA polymer is a more sensitive contrast agent for ^{19}F MRI as indicated by its lower detection limit compared with the PPEGA–PTFEA polymer. In addition, the PMSEA–PTFEA polymers displayed no obvious cytotoxicity according to cell viability studies, enabling further biological applications. Preliminary animal experiments revealed that the PMSEA–PTFEA polymers can be clearly detected by ^{19}F MRI within a short scanning time (~ 13 min), demonstrating the potential of these polymers being used as highly sensitive ^{19}F imaging agents for further *in vivo* experiments.

EXPERIMENTAL SECTION

Materials. 2-(Methylthio)ethanol (99%), 2,2,2-trifluoroethyl acrylate (TFEA, 99%), acryloyl chloride (97%), poly(ethylene glycol) methyl ether acrylate average $M_n = 480$ (PEGA), hydrogen peroxide solution (30%, w/w in H_2O), and azobis(isobutyronitrile) (AIBN) were purchased from Sigma-Aldrich and used as received. 2-(*n*-Butyltrithiocarbonate)propionic acid (BTPA) was synthesized according to previous literature.⁴⁶

Synthesis of 2-(Methylthio)ethyl Acrylate. 2-(Methylthio)ethanol (2.5 g, 2.71 mmol) and triethylamine (3.0 g, 2.97 mmol) were dissolved in 50 mL of THF in a 100 mL round-bottom flask cooled in an ice bath. Acryloyl chloride (3.1 g, 3.43 mmol) was added dropwise with stirring. After addition, the flask was removed from ice bath and left at room temperature for 12 h. After removal of white solid by filtration and THF by rotary evaporation, the crude product was purified by silica gel column with ethyl acetate/*n*-hexane (1:10, v/v) as the mobile phase, producing a colorless liquid as product (yield $\sim 64\%$). ^1H NMR (400 MHz, CDCl_3)/ppm: 6.36 (dd, 1H, vinyl), 6.10 (dd, 1H, vinyl), 5.79 (dd, 1H, vinyl), 4.27 (t, 2H, OCH_2CH_2), 2.70 (t, 2H, OCH_2CH_2), 2.10 (s, 3H, SCH_3).

Synthesis of 2-(Methylsulfinyl)ethyl Acrylate. 2-(Methylthio)ethyl acrylate (2.5 g, 17.1 mmol) and H_2O_2 (0.64 g, 18.8 mmol) were mixed in 15 mL of acetone and reacted at room temperature for 48 h. Afterward, the acetone was removed by rotary evaporation. The product was extracted by DCM and then purified by silica gel column with a mixture of methanol and *n*-hexane (1:5, v/v) as the eluent. The product was obtained as a pale yellow liquid (yield $\sim 87\%$). ^1H NMR (400 MHz, CDCl_3)/ppm: 6.40 (dd, 1H, vinyl), 6.10 (dd, 1H, vinyl), 5.81 (dd, 1H, vinyl), 4.51 (m, 2H, OCH_2CH_2), 2.98 (m, 2H, OCH_2CH_2), 2.60 (s, 3H, SOCH_3). ^{13}C NMR (100 MHz, CDCl_3)/ppm: 165.57, 131.82, 127.64, 57.21, 53.43, 39.02. ESI-MS: expected (185.02); found (185.16).

Synthesis of PMSEA–PTFEA Polymers via RAFT Polymerization. A typical procedure for RAFT polymerization of MSEA and TFEA for the synthesis of PMSEA–PTFEA polymers was as follows:

BTPA (31 mg, 0.13 mmol), MSEA (420 mg, 2.60 mmol), TFEA (100 mg, 0.65 mmol), AIBN (4.2 mg, 0.026 mmol), and 1 mL of DMF were placed into a 20 mL tube. The tube was then sealed with rubber septum followed by degassing the solution for 15 min using argon. Then the solution was put into an oil bath at 70 °C. Several aliquots were withdrawn at desired intervals of time for GPC and NMR analysis to obtain the kinetics of polymerization. The total monomer conversions were calculated from the NMR spectra using the following equation: $\alpha = (1 - (I^{6.33-6.15 \text{ ppm}} / (I^{4.46-4.20 \text{ ppm}} / 2))) \times 100\%$. The conversion of MSEA was calculated using the following equation: $\beta = (1 - (I^{5.70-5.62 \text{ ppm}} / (I^{2.51-2.40 \text{ ppm}} / 3))) \times 100\%$. The conversion of TFEA was calculated using the following equation: $\gamma = (1 - (I^{5.80-5.73 \text{ ppm}} / (I^{4.46-4.20 \text{ ppm}} / 2 - I^{2.51-2.40 \text{ ppm}} / 3))) \times 100\%$. The mole fraction of TFEA in the polymer (purified) was calculated using the following equation: $\theta = (1 - (I^{3.18-2.80 \text{ ppm}} / 2) / (I^{4.61-4.23 \text{ ppm}} / 2)) \times 100\%$. The polymerization was quenched by exposure to air. The polymer was purified by precipitation of polymer solution into diethyl ether for three times followed by being dried under vacuum.

All the other polymers were synthesized in a similar manner.

Size Exclusion Chromatography (SEC). The number-average molecular weight (M_n) and molecular weight distribution (molar mass dispersity, $D = M_w/M_n$) of the polymers were determined by SEC using a Waters Alliance 2690 separation module equipped with a Waters 2414 differential refractive index (RI) detector, a Waters 2489 UV/vis detector, a Waters 717 Plus autosampler, and a Waters 1515 isocratic HPLC pump. DMAc was used as the mobile phase with a flow rate of 1 mL/min. The system was calibrated using polystyrene standards with molecular weights ranging from 6.82×10^2 to 1.67×10^6 g/mol. The polymers were dissolved in DMAc, filtered through a PTFE membrane (0.45 μm pore size), and then subjected to injection. The PPEGA-PTFEA polymers were characterized by THF GPC with a similar instrument setup.

^1H and ^{13}C Nuclear Magnetic Resonance (NMR). ^1H NMR, ^{13}C NMR, and ^1H diffusion-ordered spectroscopy (^1H DOSY) spectra were performed on a Bruker Avance 400 MHz spectrometer at 25 °C. The solvent was deuterated chloroform (CDCl_3) or $\text{PBS}/\text{D}_2\text{O}$ (90/10, v/v). All chemical shifts are reported in ppm (δ) relative to tetramethylsilane (TMS).

^{19}F Nuclear Magnetic Resonance (^{19}F NMR). ^{19}F NMR spectra were acquired using a Bruker Avance 400 MHz spectrometer with $\text{PBS}/\text{D}_2\text{O}$ (90/10, v/v) as solvent. Solution spectra were measured under the following measurements conditions: 90° pulse width 15 μs , relaxation delay 2 s, acquisition time 0.73 s, and 32 scans.

Spin-Spin Relaxation Times (T_2). The T_2 times of polymers were measured using the Carr-Purcell-Meiboom-Gill (CPMG) pulse sequence at 298 K. The relaxation delay was 1 s, and the number of scans was 64. The samples were dissolved in a mixture of $\text{PBS}/\text{D}_2\text{O}$ (90/10, v/v) with a concentration of 10 mg/mL. For each measurement, the echo times were from 2 to 770 ms, and 16 points were collected. The decay in amplitude of the spin echo could be described by a single-exponential function, allowing the calculation of T_2 .

Spin-Lattice Relaxation Times (T_1). The T_1 times were measured using the standard inversion-recovery pulse sequence. The samples were dissolved in a mixture of $\text{PBS}/\text{D}_2\text{O}$ (90/10, v/v) with a concentration of 10 mg/mL. For each measurement, the relaxation delay was 2 s and the number of scans was 32.

^{19}F MRI Imaging. Images of phantoms containing the polymer solutions were acquired on a Bruker BioSpec 94/30 USR 9.4 T small animal MRI scanner. Polymer solutions were loaded in 5 mm NMR tubes, which were placed in a $^1\text{H}/^{19}\text{F}$ dual resonator 40 mm volume coil. ^1H MRI images were acquired for localization of the samples using a rapid acquisition with relaxation enhancement (RARE) sequence (rare factor = 16, TE = 15.4 ms, TR = 1500 ms, FOV = 30×30 mm, matrix = 256×256). ^{19}F MRI images were acquired in the same stereotactic space as the ^1H image using the RARE sequence (rare factor = 32, TE = 15.4 ms, TR = 1500 ms, FOV = 30×30 mm, matrix = 64×64 , scan time = 51 min 12 s).

For the animal experiments, ^1H MRI images were acquired using same RARE sequence (rare factor = 16, TE = 15.4 ms, TR = 1500 ms,

FOV = 60×60 mm, matrix = 256×256). ^{19}F MRI images were acquired using the RARE sequence (rare factor = 32, TE = 10 ms, TR = 1500 ms, FOV = 60×60 mm, matrix = 32×32 , scan time = 12 min 48 s).

Dynamic Light Scattering (DLS) and Zeta Potential. DLS and zeta potential measurements were conducted using a Malvern Instrument Zetasizer nano series instrument equipped with a 4.0 mW He-Ne laser operating at 633 nm and a detection angle of 173°. The number-weighted hydrodynamic diameter was obtained from analysis of the autocorrelation functions using the method of cumulants. At least three measurements at 25 °C were made for each sample with an equilibrium time of 2 min before starting measurement. The concentration of polymers was 10 mg/mL in PBS.

Cytotoxicity Studies. CHO cells were seeded into 96-well plate at a density of 10000 cells per well. After 48 h incubation, the cells were treated with different concentrations of polymer (0, 0.125, 0.25, 0.5, 1, and 2 mg/mL). After 24 h incubation, cells were treated with PrestoBlue cell viability reagent for 30 min, and the cell viability was detected by measuring the fluorescence intensity using a microplate reader Tecan X200 with excitation wavelength of 560 nm and emission wavelength of 590 nm. The fluorescence of 0 mg/mL sample was determined as 100% cell viability. Data are presented as mean \pm standard deviation (SD), $n = 5$.

In Vivo Experiments. Mouse experiments were performed using Female Balb/c nu/nu mice that were bred at the University of Queensland animal house. The mice were 10 weeks old for all experiments. Experiments were repeated three times. Prior to imaging experiments, 200 μL of polymer solution (40 mg/mL in PBS) was injected to the mice through the tail vein. MRI images of live mice were taken at predetermined times on a Bruker BioSpec 94/30 USR 9.4 T small animal MRI scanner. Ethical clearance was obtained from the University of Queensland for live mice testing (AIBN/338/16). The respiration rate of the mouse was monitored at all times during the imaging experiment. The mouse was anaesthetized with an IP injection of 65 mg/kg ketamine, 13 mg/kg xylazine, and 1.5 mg/kg acepromazine.

■ ASSOCIATED CONTENT

📄 Supporting Information

The Supporting Information is available free of charge on the ACS Publications website at DOI: 10.1021/acs.macromol.8b01190.

Figures S1 and S2 (PDF)

■ AUTHOR INFORMATION

Corresponding Author

*E-mail: a.whittaker@uq.edu.au (A.K.W.).

ORCID

Hang Ta: 0000-0003-1188-0472

Andrew K. Whittaker: 0000-0002-1948-8355

Notes

The authors declare no competing financial interest.

■ ACKNOWLEDGMENTS

A.W. acknowledges the financial support from Australian Research Council (CE140100036, DP0987407, DP110104299, DP180101221, LE0775684, LE0668517, and LE0882357) and the National Health and Medical Research Council (APP1021759). C.F. acknowledges the University of Queensland for a UQ Development Fellowship (UQFEL1831361). The Australian National Fabrication Facility, Queensland Node, is also acknowledged for access to some equipment.

REFERENCES

- (1) Huettel, S. A.; Song, A. W.; McCarthy, G. *Functional Magnetic Resonance Imaging*; Sinauer Associates: Sunderland, 2004; Vol. 1.
- (2) Flacke, S.; Fischer, S.; Scott, M. J.; Fuhrhop, R. J.; Allen, J. S.; McLean, M.; Winter, P.; Sicard, G. A.; Gaffney, P. J.; Wickline, S. A.; Lanza, G. M. Novel MRI contrast agent for molecular imaging of fibrin: implications for detecting vulnerable plaques. *Circulation* **2001**, *104*, 1280–1285.
- (3) Caravan, P.; Ellison, J. J.; McMurry, T. J.; Lauffer, R. B. Gadolinium (III) chelates as MRI contrast agents: structure, dynamics, and applications. *Chem. Rev.* **1999**, *99*, 2293–2352.
- (4) Na, H. B.; Song, I. C.; Hyeon, T. Inorganic nanoparticles for MRI contrast agents. *Adv. Mater.* **2009**, *21*, 2133–2148.
- (5) Park, J. Y.; Baek, M. J.; Choi, E. S.; Woo, S.; Kim, J. H.; Kim, T. J.; Jung, J. C.; Chae, K. S.; Chang, Y.; Lee, G. H. Paramagnetic ultrasmall gadolinium oxide nanoparticles as advanced T₁ MRI contrast agent: account for large longitudinal relaxivity, optimal particle diameter, and in vivo T₁ MR images. *ACS Nano* **2009**, *3*, 3663–3669.
- (6) High, W. A.; Ayers, R. A.; Chandler, J.; Zito, G.; Cowper, S. E. Gadolinium is detectable within the tissue of patients with nephrogenic systemic fibrosis. *J. Am. Acad. Dermatol.* **2007**, *56*, 21–26.
- (7) Broome, D. R.; Girguis, M. S.; Baron, P. W.; Cottrell, A. C.; Kjellin, I.; Kirk, G. A. Gadodiamide-associated nephrogenic systemic fibrosis: why radiologists should be concerned. *AJR, Am. J. Roentgenol.* **2007**, *188*, 586–592.
- (8) <https://www.fda.gov/Safety/MedWatch/SafetyInformation/SafetyAlertsforHumanMedicalProducts/ucm589580.htm>.
- (9) Reineri, F.; Viale, A.; Giovenzana, G.; Santelia, D.; Dastru, W.; Gobetto, R.; Aime, S. New hyperpolarized contrast agents for 13C-MRI from para-hydrogenation of oligoalkoxyethylene alkynes. *J. Am. Chem. Soc.* **2008**, *130*, 15047–15053.
- (10) Utsumi, H.; Yamada, K.-i.; Ichikawa, K.; Sakai, K.; Kinoshita, Y.; Matsumoto, S.; Nagai, M. Simultaneous molecular imaging of redox reactions monitored by Overhauser-enhanced MRI with ¹⁴N- and ¹⁵N-labeled nitroxyl radicals. *Proc. Natl. Acad. Sci. U. S. A.* **2006**, *103*, 1463–1468.
- (11) Yamada, H.; Hasegawa, Y.; Imai, H.; Takayama, Y.; Sugihara, F.; Matsuda, T.; Tochio, H.; Shirakawa, M.; Sando, S.; Kimura, Y.; et al. Magnetic resonance imaging of tumor with a self-traceable phosphorylcholine polymer. *J. Am. Chem. Soc.* **2015**, *137*, 799–806.
- (12) Ouwerkerk, R.; Morgan, R. H. ²³Na MRI: from research to clinical use. *J. Am. Coll. Radiol.* **2007**, *4*, 739–741.
- (13) Tirotta, I.; Dichiarante, V.; Pigliacelli, C.; Cavallo, G.; Terraneo, G.; Bombelli, F. B.; Metrangolo, P.; Resnati, G. 19F magnetic resonance imaging (MRI): from design of materials to clinical applications. *Chem. Rev.* **2015**, *115*, 1106–1129.
- (14) Knight, J. C.; Edwards, P. G.; Paisey, S. J. Fluorinated contrast agents for magnetic resonance imaging; a review of recent developments. *RSC Adv.* **2011**, *1*, 1415–1425.
- (15) Du, W.; Nyström, A. M.; Zhang, L.; Powell, K. T.; Li, Y.; Cheng, C.; Wickline, S. A.; Wooley, K. L. Amphiphilic hyperbranched fluoropolymers as nanoscopic 19F magnetic resonance imaging agent assemblies. *Biomacromolecules* **2008**, *9*, 2826–2833.
- (16) Fu, C.; Bongers, A.; Wang, K.; Yang, B.; Zhao, Y.; Wu, H.; Wei, Y.; Duong, H. T.; Wang, Z.; Tao, L. Facile synthesis of a multifunctional copolymer via a concurrent RAFT-enzymatic system for theranostic applications. *Polym. Chem.* **2016**, *7*, 546–552.
- (17) Xie, D.; King, T. L.; Banerjee, A.; Kohli, V.; Que, E. L. Exploiting copper redox for 19F magnetic resonance-based detection of cellular hypoxia. *J. Am. Chem. Soc.* **2016**, *138*, 2937–2940.
- (18) Xie, D.; Kim, S.; Kohli, V.; Banerjee, A.; Yu, M.; Enriquez, J. S.; Luci, J. J.; Que, E. L. Hypoxia-Responsive 19F MRI Probes with Improved Redox Properties and Biocompatibility. *Inorg. Chem.* **2017**, *56*, 6429–6437.
- (19) Shin, S. H.; Park, E.-J.; Min, C.; Choi, S. I.; Jeon, S.; Kim, Y.-H.; Kim, D. Tracking perfluorocarbon nanoemulsion delivery by 19F MRI for precise high intensity focused ultrasound tumor ablation. *Theranostics* **2017**, *7*, 562–572.
- (20) Srinivas, M.; Boehm-Sturm, P.; Figdor, C. G.; de Vries, I. J.; Hoehn, M. Labeling cells for in vivo tracking using 19F MRI. *Biomaterials* **2012**, *33*, 8830–8840.
- (21) Gaudet, J. M.; Ribot, E. J.; Chen, Y.; Gilbert, K. M.; Foster, P. J. Tracking the fate of stem cell implants with fluorine-19 MRI. *PLoS One* **2015**, *10*, e0118544.
- (22) Peng, H.; Blakey, I.; Dargaville, B.; Rasoul, F.; Rose, S.; Whittaker, A. K. Synthesis and evaluation of partly fluorinated block copolymers as MRI imaging agents. *Biomacromolecules* **2009**, *10*, 374–381.
- (23) Kislukhin, A. A.; Xu, H.; Adams, S. R.; Narsinh, K. H.; Tsien, R. Y.; Ahrens, E. T. Paramagnetic fluorinated nanoemulsions for sensitive cellular fluorine-19 magnetic resonance imaging. *Nat. Mater.* **2016**, *15*, 662–668.
- (24) Zhang, C.; Moonshi, S. S.; Han, Y.; Puttick, S.; Peng, H.; Magoling, B. J. A.; Reid, J. C.; Bernardi, S.; Searles, D. J.; Král, P.; Whittaker, A. K. PFPE-Based Polymeric 19F MRI Agents: A New Class of Contrast Agents with Outstanding Sensitivity. *Macromolecules* **2017**, *50*, 5953–5963.
- (25) Moonshi, S. S.; Zhang, C.; Peng, H.; Puttick, S.; Rose, S.; Fisk, N. M.; Bhakoo, K.; Stringer, B. W.; Qiao, G. G.; Gurr, P. A.; Whittaker, A. K. A unique 19 F MRI agent for the tracking of non phagocytic cells in vivo. *Nanoscale* **2018**, *10*, 8226–8239.
- (26) Grapentin, C.; Barnert, S.; Schubert, R. Monitoring the stability of perfluorocarbon nanoemulsions by Cryo-TEM image analysis and dynamic light scattering. *PLoS One* **2015**, *10*, e0130674.
- (27) Jacoby, C.; Temme, S.; Mayenfels, F.; Benoit, N.; Krafft, M. P.; Schubert, R.; Schrader, J.; Flögel, U. Probing different perfluorocarbons for in vivo inflammation imaging by 19F MRI: image reconstruction, biological half-lives and sensitivity. *NMR Biomed.* **2014**, *27*, 261–271.
- (28) Kirberger, S. E.; Maltseva, S. D.; Manulik, J. C.; Einstein, S. A.; Weegman, B. P.; Garwood, M.; Pomerantz, W. C. Synthesis of Intrinsically Disordered Fluorinated Peptides for Modular Design of High-Signal 19F MRI Agents. *Angew. Chem., Int. Ed.* **2017**, *56*, 6440–6444.
- (29) Preslar, A. T.; Tantakitti, F.; Park, K.; Zhang, S.; Stupp, S. I.; Meade, T. J. 19F Magnetic Resonance Imaging Signals from Peptide Amphiphile Nanostructures Are Strongly Affected by Their Shape. *ACS Nano* **2016**, *10*, 7376–7384.
- (30) Wallat, J. D.; Czapar, A. E.; Wang, C.; Wen, A. M.; Wek, K. S.; Yu, X.; Steinmetz, N. F.; Pokorski, J. K. Optical and Magnetic Resonance Imaging Using Fluorous Colloidal Nanoparticles. *Biomacromolecules* **2017**, *18*, 103–112.
- (31) Wang, K.; Peng, H.; Thurecht, K. J.; Puttick, S.; Whittaker, A. K. Segmented highly branched copolymers: Rationally designed macromolecules for improved and tunable 19f mri. *Biomacromolecules* **2015**, *16*, 2827–2839.
- (32) Fu, C.; Herbst, S.; Zhang, C.; Whittaker, A. K. Polymeric 19 F MRI agents responsive to reactive oxygen species. *Polym. Chem.* **2017**, *8*, 4585–4595.
- (33) Thurecht, K. J.; Blakey, I.; Peng, H.; Squires, O.; Hsu, S.; Alexander, C.; Whittaker, A. K. Functional hyperbranched polymers: toward targeted in vivo 19F magnetic resonance imaging using designed macromolecules. *J. Am. Chem. Soc.* **2010**, *132*, 5336–5337.
- (34) Rolfe, B. E.; Blakey, I.; Squires, O.; Peng, H.; Boase, N. R.; Alexander, C.; Parsons, P. G.; Boyle, G. M.; Whittaker, A. K.; Thurecht, K. J. Multimodal polymer nanoparticles with combined 19F magnetic resonance and optical detection for tunable, targeted, multimodal imaging in vivo. *J. Am. Chem. Soc.* **2014**, *136*, 2413–2419.
- (35) Zhao, W.; Ta, H. T.; Zhang, C.; Whittaker, A. K. Polymerization-Induced Self-Assembly (PISA)-Control over the Morphology of 19F-Containing Polymeric Nano-objects for Cell Uptake and Tracking. *Biomacromolecules* **2017**, *18*, 1145–1156.
- (36) Li, S.; Chung, H. S.; Simakova, A.; Wang, Z.; Park, S.; Fu, L.; Cohen-Karni, D.; Averick, S.; Matyjaszewski, K. Biocompatible

polymeric analogues of DMSO prepared by atom transfer radical polymerization. *Biomacromolecules* **2017**, *18*, 475–482.

(37) Oyama, T.; Naka, K.; Chujo, Y. Polymer Homologue of DMSO: Synthesis of Poly (ethylene sulfoxide) by Selective Oxidation of Poly (ethylene sulfide). *Macromolecules* **1999**, *32*, 5240–5242.

(38) Herzberger, J.; Fischer, K.; Leibig, D.; Bros, M.; Thiermann, R.; Frey, H. Oxidation-responsive and “clickable” poly (ethylene glycol) via copolymerization of 2-(methylthio) ethyl glycidyl ether. *J. Am. Chem. Soc.* **2016**, *138*, 9212–9223.

(39) Xu, S.; Ng, G.; Xu, J.; Kuchel, R. P.; Yeow, J.; Boyer, C. 2-(Methylthio) ethyl Methacrylate: A Versatile Monomer for Stimuli Responsiveness and Polymerization-Induced Self-Assembly in the Presence of Air. *ACS Macro Lett.* **2017**, *6*, 1237–1244.

(40) Xiao, C.; Ding, J.; Ma, L.; Yang, C.; Zhuang, X.; Chen, X. Synthesis of thermal and oxidation dual responsive polymers for reactive oxygen species (ROS)-triggered drug release. *Polym. Chem.* **2015**, *6*, 738–747.

(41) Napoli, A.; Valentini, M.; Tirelli, N.; Müller, M.; Hubbell, J. A. Oxidation-responsive polymeric vesicles. *Nat. Mater.* **2004**, *3*, 183–189.

(42) Rodriguez, A. R.; Kramer, J. R.; Deming, T. J. Enzyme-triggered cargo release from methionine sulfoxide containing copolypeptide vesicles. *Biomacromolecules* **2013**, *14*, 3610–3614.

(43) Ozden-Yenigun, E.; Simsek, E.; Menciloglu, Y. Z.; Atilgan, C. Molecular basis for solvent dependent morphologies observed on electrosprayed surfaces. *Phys. Chem. Chem. Phys.* **2013**, *15*, 17862–17872.

(44) Taylor, A. J.; Granwehr, J.; Lesbats, C.; Krupa, J. L.; Six, J. S.; Pavlovskaya, G. E.; Thomas, N. R.; Auer, D. P.; Meersmann, T.; Faas, H. M. Probe-Specific Procedure to Estimate Sensitivity and Detection Limits for 19F Magnetic Resonance Imaging. *PLoS One* **2016**, *11*, e0163704.

(45) Boehm-Sturm, P.; Mengler, L.; Wecker, S.; Hoehn, M.; Kallur, T. In vivo tracking of human neural stem cells with 19F magnetic resonance imaging. *PLoS One* **2011**, *6*, e29040.

(46) Fu, C.; Xu, J.; Kokotovic, M.; Boyer, C. One-pot synthesis of block copolymers by orthogonal ring-opening polymerization and PET-RAFT polymerization at ambient temperature. *ACS Macro Lett.* **2016**, *5*, 444–449.

Enhanced Performance of Polymeric ^{19}F MRI Contrast Agents through Incorporation of Highly Water Soluble Monomer MSEA

Changkui Fu, Cheng Zhang, Hui Peng, Felicity Han, Carly Baker, Yuao Wu, Hang Ta,

Andrew K. Whittaker*

Supporting information

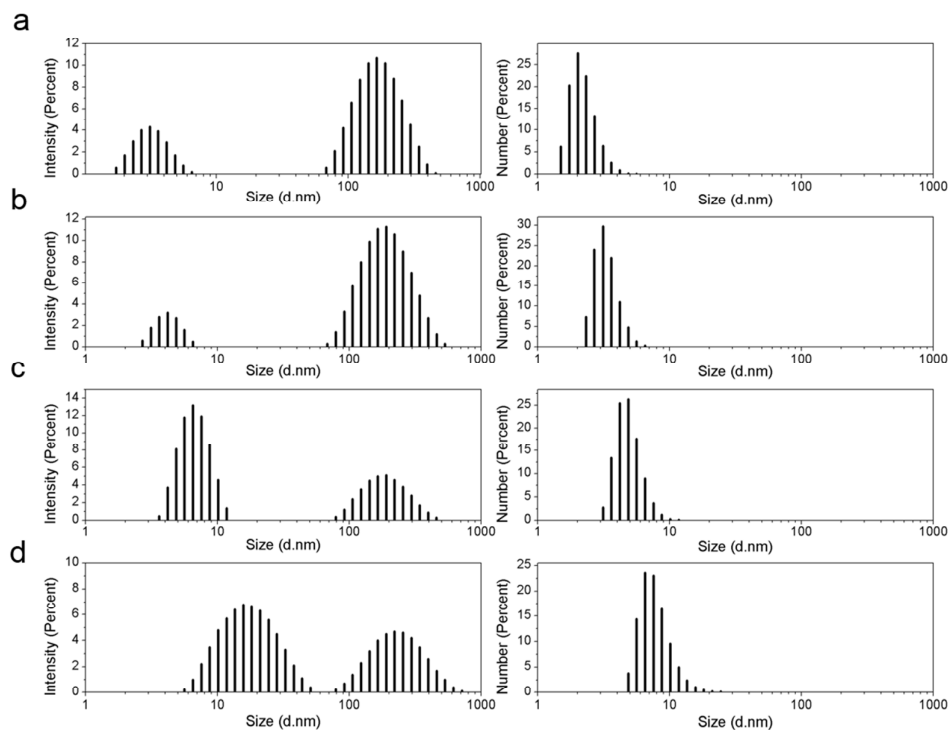


Figure S1. Results of DLS study of solutions of PMSEA-PTFEA polymers with fluorine content of (a) 5.8 wt%; (b) 9.7 wt%; (c) 15.3 wt%; (d) 19.3 wt%. Polymer concentration = 10 mg/mL in PBS.

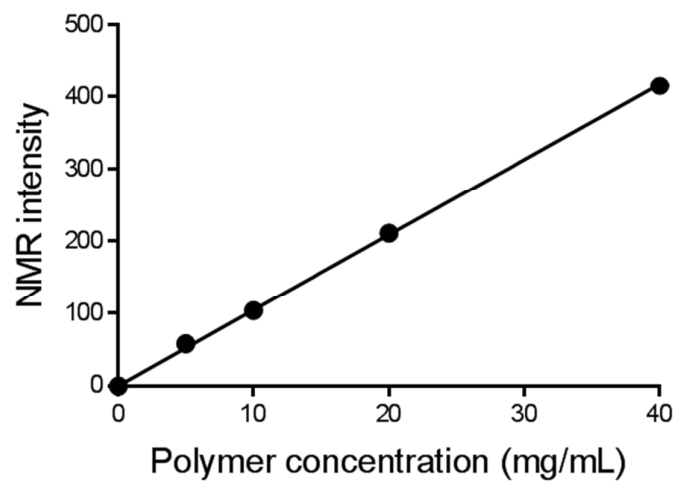


Figure S2. The linear relationship between ^{19}F NMR intensity and concentration of polymer in solution.